Graft Polymerization Synthesis and Application of Magnetic Fe$_3$O$_4$/Polyacrylic Acid Composite Nanoparticles

R. Y. Hong,[1,2,3] **T. T. Pan,**[1,2] **Y. P. Han,**[1,2] **S. Z. Zhang,**[1,2] **H. Z. Li,**[3] **J. Ding**[4]

[1]Department of Chemical Engineering, Soochow University, Suzhou 215123, China
[2]Key Laboratory of Organic Synthesis of Jiangsu Province, Soochow University, Suzhou 215006, China
[3]Key Laboratory of Multiphase Reaction, Institute of Process Engineering, Chinese Academy of Sciences, Beijing 100080, China
[4]IBM, HYDA/050-3 C202, Rochester, Minnesota 55901

ABSTRACT: Fe$_3$O$_4$ magnetic nanoparticles were prepared by coprecipitation using NH$_3$ · H$_2$O as the precipitating agent, and were characterized by Fourier transform infrared spectroscopy (FTIR), transmission electron microscopy (TEM), and X-ray powder diffraction (XRD). The compatibility between the Fe$_3$O$_4$ nanoparticles and water were enhanced by grafting acrylic acid onto the nanoparticle surface. FTIR, XRD, thermogravimetry (TG), and differential scanning calorimetry (DSC) were used to characterize the resultant sample. The effects of initiator dosage, monomer concentration, and reaction temperature on the characteristics of surface-modified Fe$_3$O$_4$ nanoparticles were investigated. Moreover, magnetic fluids (MF), prepared by dispersing the PAA grafted Fe$_3$O$_4$ nanoparticles in water, were characterized using UV–vis spectrophotometer, Gouy magnetic balance, and laser particle-size analyzer. The rheological characteristics of magnetic fluid were investigated using capillary and rotating rheometers. The MF was added to prepare PVA thin film to improve mechanical properties. © 2007 Wiley Periodicals, Inc. J Appl Polym Sci 106: 1439–1447, 2007

Key words: Fe$_3$O$_4$ nanoparticles; graft polymerization; surface modification; acrylic acid; magnetic fluid

INTRODUCTION

In recent years, nanoscaled magnetic particles have attracted much attention. These nanocrystallined particles with a high surface/volume ratio possess some extraordinary physical and chemical properties.[1] Therefore, magnetic nanoparticles can be applied to many industrial and biological fields, such as improved MRI diagnostic contrast agents, cell separation, tumor hyperthermia, retinal detachment therapy, and magnetic field-guided carriers for localizing drugs or radioactive therapies.[2] Magnetite

Fe$_3$O$_4$ powders, which are nontoxic and are easily to be synthesized, has been intensively investigated. The preparation methods of magnetite Fe$_3$O$_4$ powders mainly include coprecipitation,[3,4] microwave thermal hydrolysis,[5] plasma thesis,[6] laser ablation,[7] micron-scale capsule,[8] and glycothermal process.[9]

The outstanding characteristics of magnetic nanoparticles are due to finite-size effect or high ratio of surface to volume. It means that control and/or tailor of the surface properties of nanoparticles are of great importance. To enhance the compatibility between magnetic Fe$_3$O$_4$ nanoparticles and water, surface modification for magnetic Fe$_3$O$_4$ nanoparticles is a necessity.

Ma et al.[3] prepared Fe$_3$O$_4$ nanoparticles coated with a near monolayer of amino silane. The monolayer has active group of —NH$_2$ that can connect biomolecules, drugs, and so on. The modified magnetic nanoparticles can be dispersed into water/solvent using surfactant to form stable colloid-magnetic fluid.

In iatrology, by applying an alternating magnetic field, medicines combined with magnetic nanoparticles accumulate around tumor cells, and can be used to destroy the tumor with less harm to human body. This methodology is recently introduced as a method for the evaluation of immunoassays.[10]

In our previous investigation,[11] magnetite Fe_3O_4 nanoparticles were synthesized by coprecipitation of Fe^{2+} and Fe^{3+} using $NH_3 \cdot H_2O$ as the precipitating agent. In the present investigation, the obtained Fe_3O_4 nanoparticles were first treated with the coupling agent, KH570, followed by radical grafting polymerization in nonaqueous system to graft the ployacrylic acid (PAA) chains onto the surface of magnetic Fe_3O_4 nanoparticles. The PAA grafted magnetic nanoparticles were dispersed in water using surfactant to form magnetic fluid, which was added to improve the mechanical properties of PVA thin film.

EXPERIMENTAL

Materials

Ferric chloride ($FeCl_3 \cdot 6H_2O$), ferrous sulfate ($FeSO_4 \cdot 7H_2O$), xylene, aqueous ammonia, ethyl alcohol, and polyvinylalcohol (PVA) were all of analytic grade. Silane coupling agent (γ-methacyloxypropyl trimethoxy silane, KH570), acrylic acid monomer, azobisisobutyronitrile (AIBN), and paraffin liquid were all of chemical grade. All the above-mentioned materials were employed directly except that AIBN was recrystallized with ethanol, and acrylic acid monomer was purified by distillation under reduced pressure.

Synthesis of magnetic nanoparticles

To synthesize Fe_3O_4 nanoparticles, the mixture of $FeCl_3$ (0.5M, 70 mL), $FeSO_4$ (0.5M, 40 mL), and paraffin liquid (5 mL) was prepared under Ar protection. The molar ratio of $FeCl_3$ to $FeSO_4$ was 1.75 to 1.10 mL of ammonia aqueous solution was then quickly charged into the solution with vigorously stirring, followed by more ammonia aqueous solution being dropped into the mixture slowly with stirring until the pH value of the solution reached 9. Thereafter, the solution was kept stirring for additional 30 min under Ar protection. The resulted black mixture was aged for one night. Finally, the precipitate was collected by filtration and washed three times with distilled water and ethanol alcohol, respectively.

Introduction of reactive groups and graft polymerization

The introduction of reactive groups onto the magnetite surfaces was achieved by the reaction between KH570 and hydroxyl groups on the surface of magnetite. Typically, 1 g of Fe_3O_4 (not dried), 1 mL of silane coupling agent, and 50 mL of xylene solution were mixed together in a flask. The mixture was stirred for 3 h at a temperature of 80°C under Ar protection. Thereafter, the graft polymerization reaction was conducted. Acrylic acid (4 mL) and 130 mg of AIBN were put in the flask with stirring under Ar protection at 55°C for 2 h. Then, the magnetite particles were centrifuged and washed with ethyl alcohol for three times.

Before the TG and FTIR tests, the resultant particles were purged with ethyl alcohol for 24 h using a Soxhlet extractor to remove the homopolymer, and were dried under vacuum for 12 h.

Preparation of magnetic fluid

To synthesize Fe_3O_4 magnetic fluid, dodecyl sodium sulfate (0.222 g, 1 wt %), Fe_3O_4 nanoparticles (13 g) that were not dried under vacuum, and deionized water (20 mL) were mixed together. The mixture was ball-milled for 2 h at room temperature. Finally, the magnetic fluid was obtained.

The samples of different concentrations for viscosity measurement were obtained via the above procedure except the volume of deionized water was changed.

Preparation of PVA thin films

The polar solvent, water was used as a cosolvent of PVA and PAA-g-Fe_3O_4 composite nanoparticles since PVA dissolves in water, and PAA-g-Fe_3O_4 nanoparticles can be effectively dispersed in water. A predetermined amount of nanoparticles (0.3 g) was dispersed in water (30 mL). The mixture was vigorously stirred at a temperature nearly 100°C until a stable nanosuspension was obtained. PVA (8 g) and defoaming agent (1 wt % in 50 mL water, Surfynol MD-20, Air Products, USA) were added to water (50 mL) with stirring at a temperature nearly 100°C, and the solution was poured into the nanosuspension with strong agitation.

Wet PVA films with a thickness of 100 ± 3 μm were prepared by coating the nanosuspension or PVA solution on a smooth plastic foil with a wet film applicator (SZQ-100, XD Env. Eng. Tech., Shanghai, China). The plastic foil was sucked uniformly on a vacuum bed to improve the reproducibility of wet film. The wet film applicator was driven by an automatic film dauber (AFA-II, XD Env. Eng. Tech., Shanghai, China) to improve the precision of film thickness.

The prepared wet films on plastic foils were then set at room temperature for 1 day, and later vacuum-dried at 100°C for 1 day to completely remove any residual water. Finally, PVA thin films with a thickness of about 30 μm were taken off. The nanoparticle content in the dried film was about 3.6 wt % based on the polymer matrices.
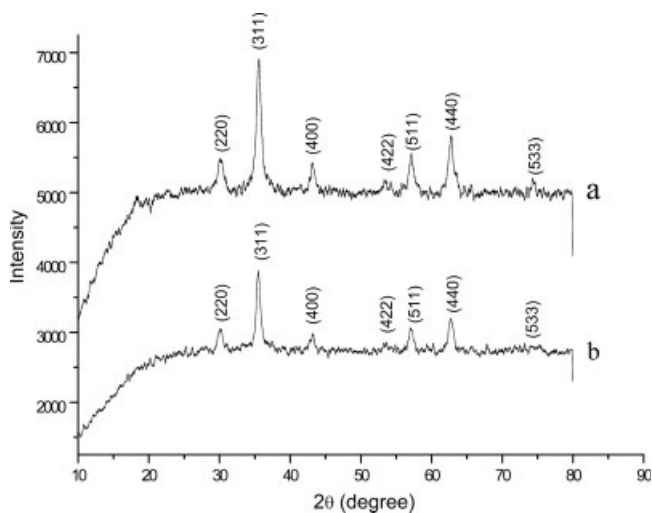
Figure 1 XRD patterns of bare Fe$_3$O$_4$ (a) and PAA-grafted Fe$_3$O$_4$ (b) nanoparticles.

The prepared thin films with almost the same thickness (20 ± 0.2 μm) were selected using a thickness gauge (No. 7327, Mitutoyo, Japan). Test samples for the stress–strain (SS) curve were cut into the shape as shown in Figure 14 according to the China National Standard, GB/T228-2002.[12]

Characterization

Fourier transform infrared (FTIR) spectra were obtained using Nicolet FTIR Avatar 360 with KBr method. The size and shape of the nanoparticles were determined by JEOL 2010 HRTEM. X-ray dif-

fraction (XRD) measurements were carried out with D/Max-IIIC, using Cu Kα radiation. PerkinElmer TGA7 and PerkinElmer DSC7 were employed to perform the thermogravimetric analysis. UV–vis spectra were achieved by HITACHI U-2810 spectrophotometer. The magnetic property of magnetic fluid was measured by Gouy magnetic balance (FD-TX-FM-A). The size of nanoparticles in magnetic fluid was obtained using Malvern HPPS5001 laser particle-size analyzer. An Anton Paar MCR301 rotating rheometer and a capillary rheometer were used to investigate the rheological properties of magnetic fluid.

The mechanical properties of prepared PVA thin films were measured on a KQL tensile tester (model 4465WDT-0.2, KQL Testing Instruments, Shenzhen, China) at room temperature. The force transducer with a precision of ±0.02‰ was made by Transcell Tech. USA. The crosshead speed was 5 mm/min during the test.

RESULTS AND DISCUSSION

X-ray powder diffraction patterns

X-ray powder diffraction patterns of bare Fe$_3$O$_4$ (a) and PAA-grafted Fe$_3$O$_4$ (b) nanoparticles are illustrated in Figure 1, respectively. It was found from (a) that there were a series of characteristic peaks at 4.810(111), 2.964(220), 2.525(311), 2.092(400), 1.717(422), 1.612(511), 1.478(440), and 1.276(533). The d values calculated from the XRD pattern were well indexed to the inverse cubic spinel phase of Fe$_3$O$_4$. The average crystallite size D, calculated using the Debye-Sherrer formula $D = K\lambda/(\beta \cos \theta)$, was roughly
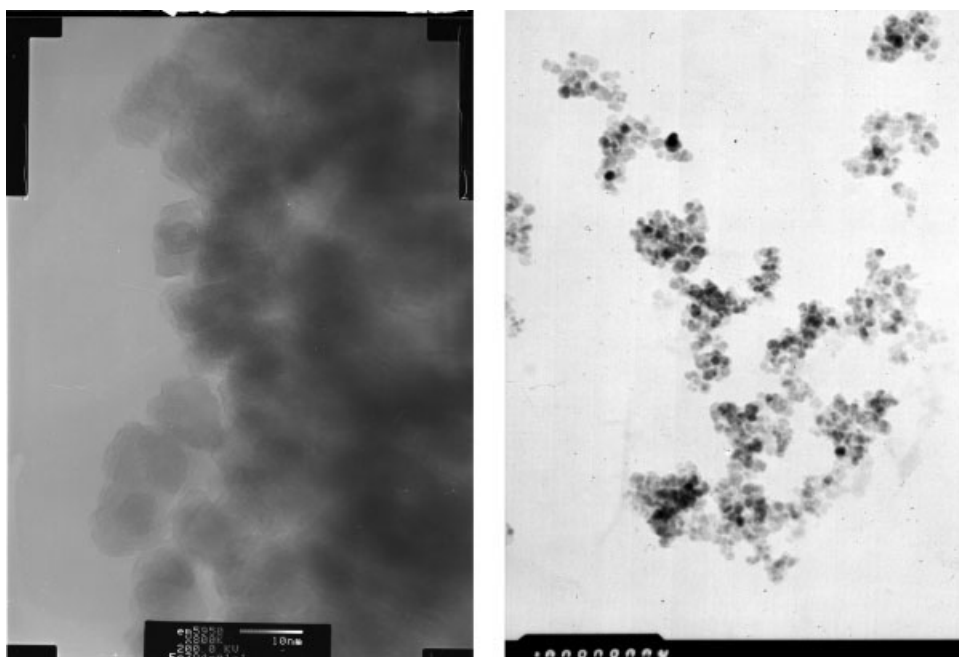

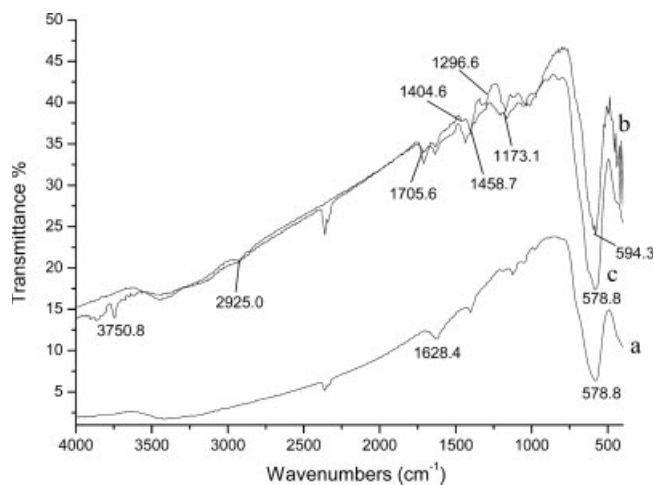**Figure 2** HRTEM of unmodified Fe$_3$O$_4$ nanoparticles.

Figure 3 FTIR spectra of (a) bare Fe_3O_4 nanoparticles; (b) Fe_3O_4 nanoparticles treated by KH570; and (c) Fe_3O_4 nanoparticles grafted by PAA.

about 10 nm. It was found from the XRD pattern of (b) that Fe_3O_4 nanoparticles treated with acrylic acid were still the inverse cubic spinel phase. Therefore, the crystal structure of Fe_3O_4 nanoparticles was not changed before and after the surface modification.

Transmission electron microscopy

Figure 2 illustrates the high-resolution transmission electron micrographs (HRTEM) of Fe_3O_4 nanoparticles, which showed that most of the particles were quasi-spherical with a diameter of around 10 nm, and the results reasonably matched with those obtained from XRD. However, because of the large specific surface area, high surface energy, and magnetization of Fe_3O_4 nanoparticles, some of the primary nanoparticles were aggregated into secondary particles during the process of drying.

FTIR spectra

Figure 3 gives the FTIR spectra of bare Fe_3O_4 (a), Fe_3O_4 treated with KH570 (b), and Fe_3O_4 grafted with PAA (c). It could be seen that, when compared with the untreated sample (a), the KH570-treated
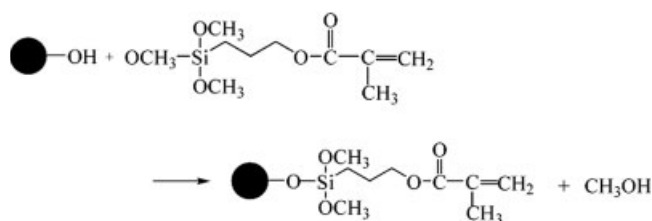

Figure 4 Schematic illustration of the reaction between the hydroxyl groups of Fe_3O_4 nanoparticles and silane-coupling agent, KH570.
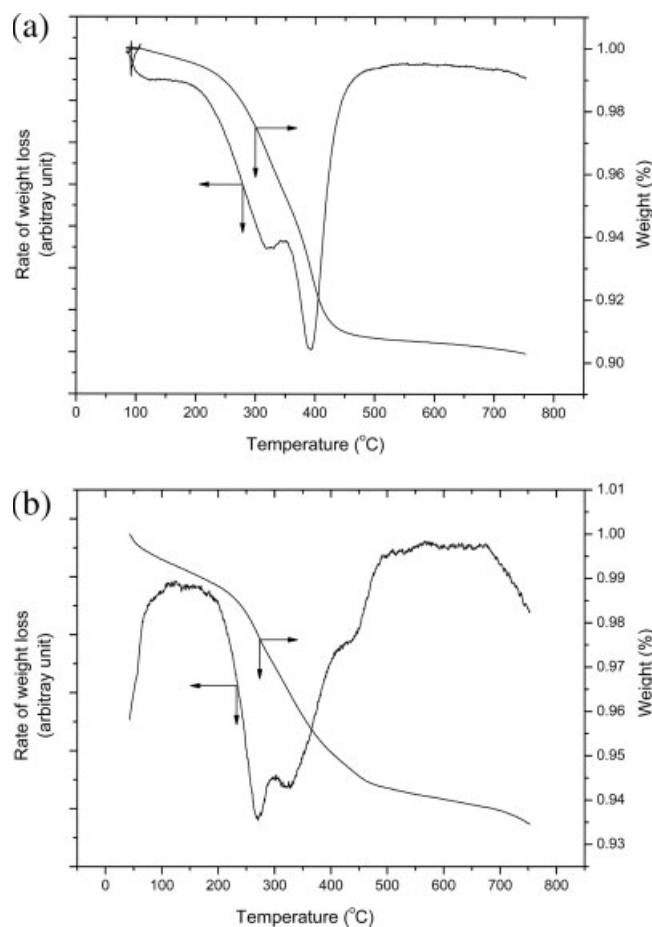
Figure 5 (a) Thermogravimetric chart of Fe_3O_4 nanoparticles grafted by PAA. (b) Thermogravimetric chart of the mixture of Fe_3O_4 nanoparticles and PAA.

Fe_3O_4 nanoparticles (b) possessed absorption band in 1404.6 cm^{-1} due to stretching vibration of Si—O bond, bands in 1296.6 and 1071.1 cm^{-1} due to stretching
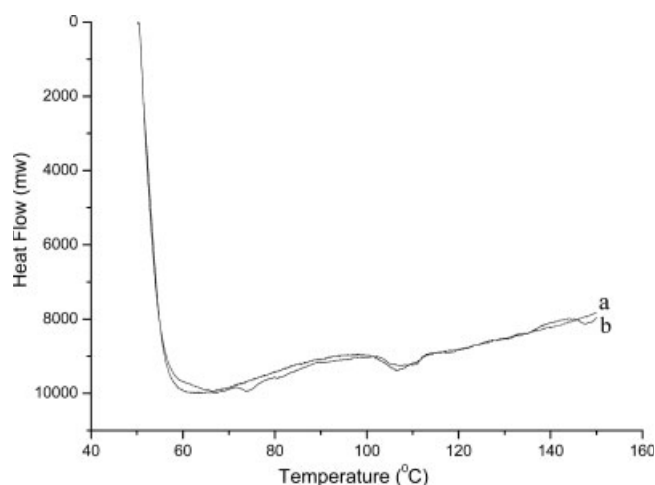

Figure 6 DSC heating curves of (a) Fe_3O_4 nanoparticles grafted by PAA and (b) the mixture of bare Fe_3O_4 nanoparticles and neat PAA.
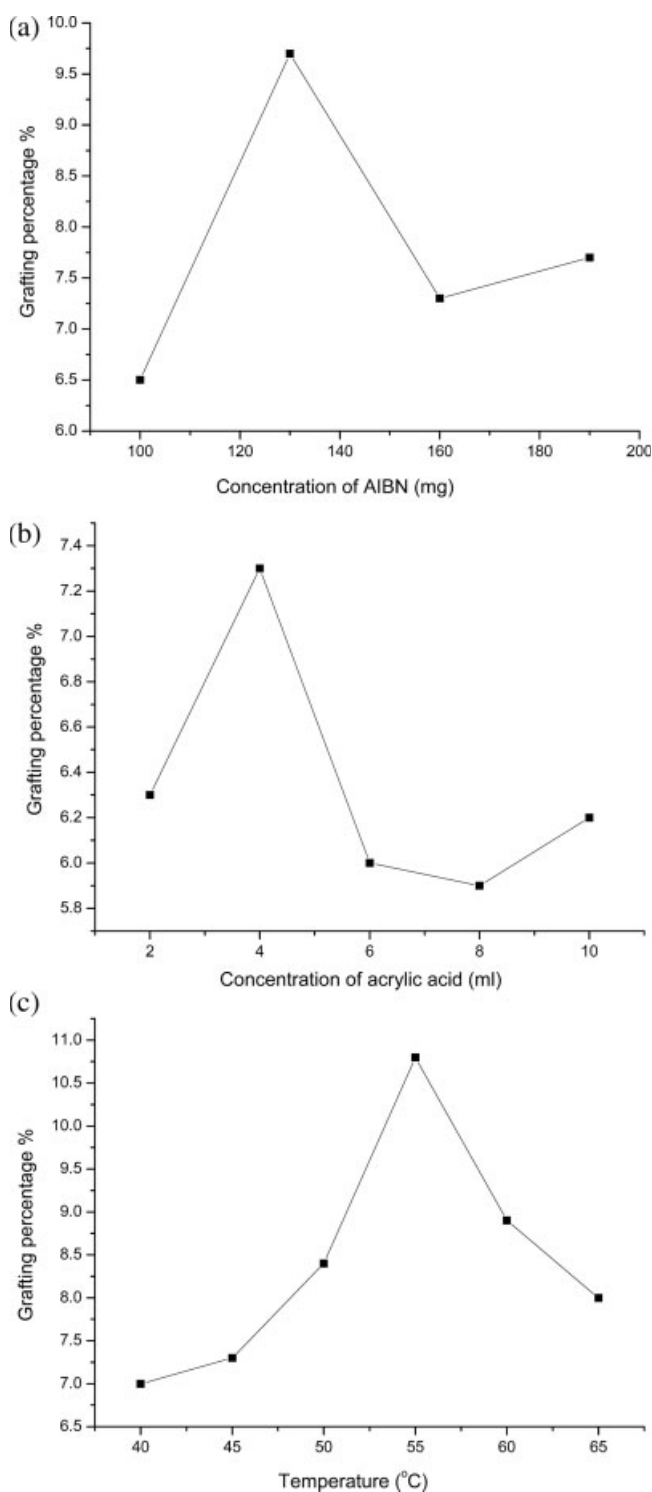
Figure 7 (a) Relationship between grafting percentage and concentration of AIBN. (b) Relationship between grafting percentage and concentration of acrylic acid. (c) Relationship between grafting percentage and reaction temperature.

vibration of C—O bond, and band in 1458.7 cm^{-1} due to bending vibration of C—H bond. All of these revealed the existence of silane-coupling agent. It indicated that the active groups had been introduced onto the surface of magnetite. The reaction mechanism was described in Figure 4. PAA-g-Fe₃O₄ nanoparticles (c) showed a new adsorption at 1705.6 cm^{-1} corresponding to C=O groups, in addition to the peak at 2925.0 cm^{-1} representing stretching vibration of C—H bond in PAA, indicating the existence of polyacrylic acid grafting chains. In these spectra, an adsorption at 578.8 or 594.3 cm^{-1} was the characteristic adsorption of Fe—O bond.

Thermogravimetric analysis

The thermogravimetric (TG) analysis of PAA-g-Fe₃O₄ nanoparticles pointed that the grafting percentage is about 13%. The TG graphs were not given here for the length limitation of the article.

TG analysis chart of Fe₃O₄ nanoparticles grafted by PAA is shown in Figure 5(a). It could be confirmed that the grafting percentage of PAA is 9.71%. The simple mixture of bare Fe₃O₄ nanoparticles and neat PAA was prepared using solution blending with a high-energy ball mill. The ball mill was operated at a rotating speed of 40 rpm. The solvent, acetone, employed during the ball milling was removed at 60°C under vacuum. When compared with the mixture of magnetite and PAA [Fig. 5(b)], it showed that there was a remarkable difference in thermal behaviors between the PAA-grafted magnetite and the mixture of magnetite and PAA. The degradation temperature of PAA-grafted magnetite was much higher than that of the mixture of magnetite and PAA. That is, the PAA grafted onto the surface of Fe₃O₄ nanoparticles has much higher thermal stability than the simple mixture of PAA and Fe₃O₄ nanoparticles. This further verifies a strong interaction between the grafting PAA and Fe₃O₄ nanoparticles.
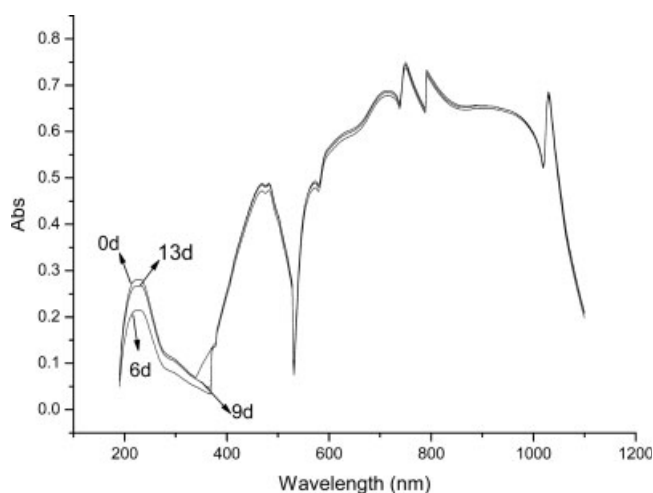

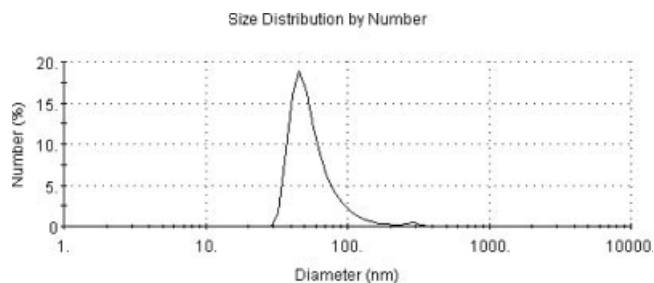**Figure 8** UV–vis spectrum of magnetic fluid under gravitational field.

Figure 9 Size distribution of Fe$_3$O$_4$ nanoparticles in magnetic fluid.

This result is in accordance with the testing results from FTIR mentioned earlier.

Figure 6 shows the DSC curves. The glass transition temperature of nanoparticles grafted by PAA (a), at 105.2°C, was a little lower than that of the mixture
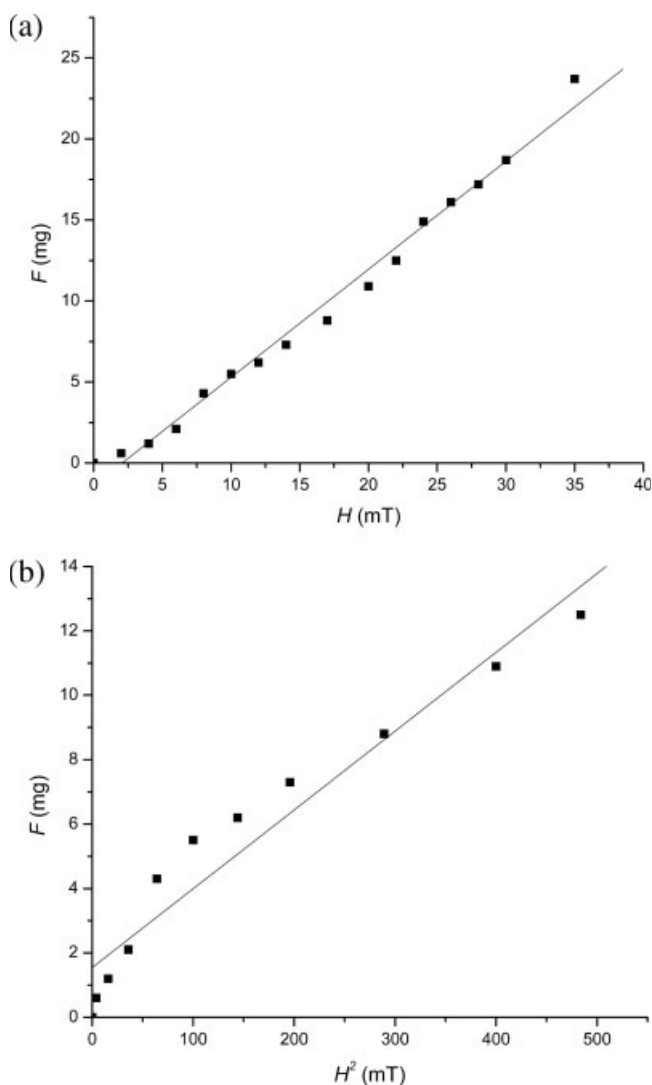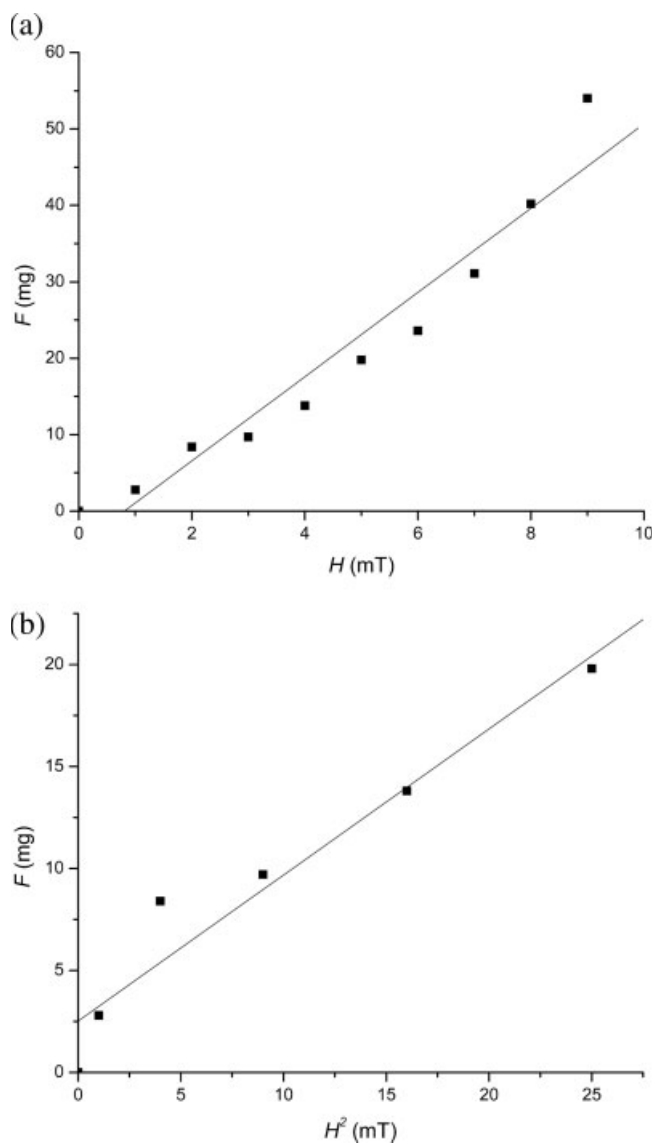

Figure 11 Relationship between the magnetic weight and magnetic field (at a weight concentration of 32.3%).

of bare magnetite and neat PAA (b) at 108.5°C. Such behavior can be explained by the restricting effect of the nanoparticles in polymer. The Fe$_3$O$_4$ nanoparticles dispersed in PAA might be able to block the movement of PAA polymer chains during DSC heating scans, and increase the glass transition temperature. The Fe$_3$O$_4$ nanoparticles grafted by PAA have less effect on the chain movement, and so the glass transition temperature of nanoparticles grafted by PAA is relatively lower.

Effects of reaction conditions

The effects of initiator dosage, concentrations of acrylic acid, and reaction temperature on graft polymerization are shown in Figure 7. The grafting percentage of PAA onto nanoparticles reaches its
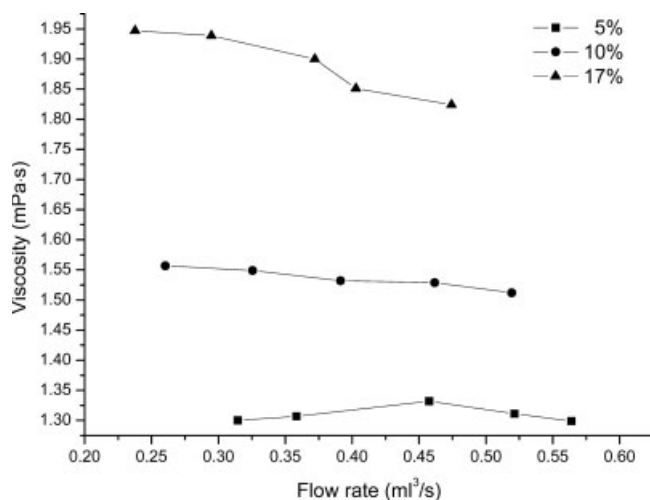

Figure 10 Relationship between the magnetic weight and magnetic field (at a weight concentration of 5%).

Figure 12 Viscosity versus flow rate at different solid concentration measured using a capillary rheometer.

Figure 13 Viscosity versus temperature measured using a rotating rheometer (A. magnetic fluid (17%, in weight); B. surfactant solution).

maximum when Fe_3O_4 nanoparticles react with 4 mL of acrylic acid and 130 mg of AIBN at 55°C.

Effect of initiator dosage

The effect of the initiator added on the grafting percentage is shown in Figure 7(a). When the concentration of initiator exceeded 130 mg, the grafting percentage of nanoparticles decreased. The results can be explained that there was a competitive reaction in the solution (grafting polymerization of acrylic acid onto Fe_3O_4 nanoparticles and polymerization of acrylic acid in the solution), and excessive amount of the initiator could increase the polymerization of acrylic acid in the solution.

Effect of acrylic acid concentration

The effect of acrylic acid concentration was investigated, and the result is shown in Figure 7(b). The grafting percentage increased with increasing monomer concentration, reached a maximum, and decreased thereafter. This was due to the long chains of polyacrylic acid, which belonged to the homopolymer synthesized in the solution, tangling on the surface of particles, and further hindered the reaction of surface grafting polymerization. The more monomers added in, the more acrylic acid wasted in side reactions. Therefore, the optimum amount of acrylic acid was selected as 4 mL.

Effect of reaction temperature

The reacting temperature greatly influences chemical reactions in most instances. Effect of polymerizing temperature on grafting percentage was investigated
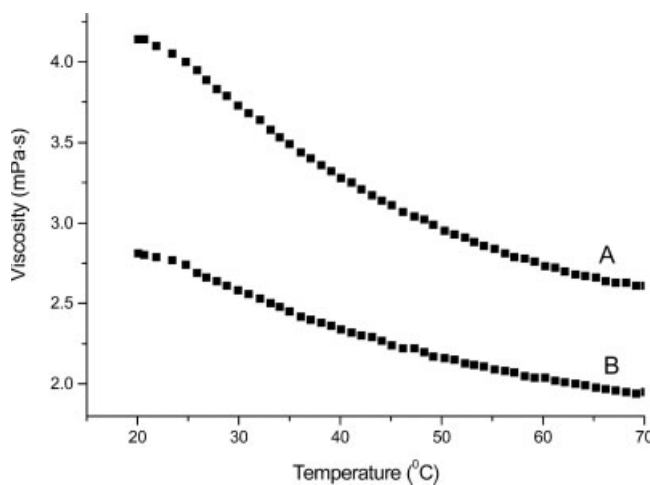
from 40 to 65°C when the reactions were carried out with the acrylic acid concentration of 4 mL and AIBN of 130 mg. The grafting percentage reached its maximum at 55°C, as shown in Figure 7(c). It was due to the fact that higher reacting temperature could improve the chain transfer reactions and also lead to more homopolymer formation.

Stability of magnetic fluid

The UV–vis absorption curves of magnetic fluid under gravitation field for 13 days are presented in Figure 8. It is shown that the absorbance of magnetic fluid almost never changed after sedimentation for 13 days, although, there was a little change between 190 and 380 nm. As shown in Figure 8, magnetic fluid exhibited excellent stability. It can be concluded that the PAA-g-Fe_3O_4 nanoparticles are able to suspend in water stably since acrylic acid has been successfully grafted onto the surfaces of Fe_3O_4 nanoparticles. The results are consistent with the FTIR spectrum of Fe_3O_4 nanoparticles coated by polyacrylic acid.
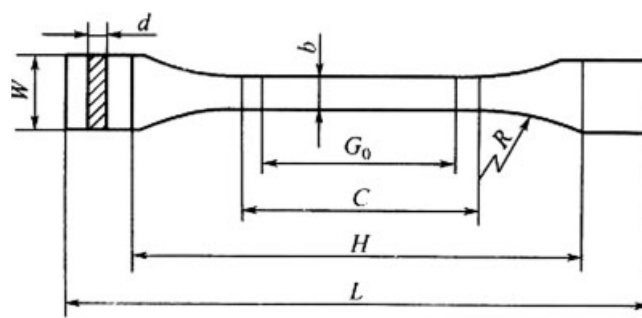

Figure 14 The shape and dimensions of the specimen.

TABLE I
The Dimensions of the Specimen (Fig. 14)

Symbol	Description	Dimension (mm)	Tolerance (mm)
L	Total length (minimum)	150	N/A
H	Distance between clamps	115	±5.0
C	Length of parallel section in the middle	60	±0.5
G_0	Length of effective part	50	±0.5
W	End width	N/A	±0.001
b	Film thickness	N/A	±0.001
R	Radius	60	±5.0

N/A, Not applicable.

Size distribution of Fe_3O_4 nanoparticles in magnetic fluid

The size distribution of PAA-g-Fe_3O_4 nanoparticles is shown in Figure 9. The number of d $(0.98)_{num}$ is 57.42 nm, meaning that the volumetric size of 98% Fe_3O_4 nanoparticles is 57.42 nm. The core size of nanoparticles calculated from HRTEM photographs in Figure 2(a) is about 10 nm, which is smaller than that of Fe_3O_4 nanoparticles in magnetic fluid. An explanation for this is that nanoparticles were wrapped by polyacrylic acid, which made these particles bigger.

Magnetic properties of magnetic fluid

PAA-g-Fe_3O_4 magnetic fluid with different concentrations can be synthesized. For the magnetic fluid at a weight concentration of 5%, the relationship between the magnetic weight and applied magnetic field is shown in Figure 10. Calculations according to the method presented in literature[13] indicated that the susceptibility of synthesized magnetic fluid was 8.17×10^{-7}, and its saturation magnetization was 17.42 mT.

For the magnetic fluid at a weight concentration of 32.3%, the relationship between the magnetic weight and applied magnetic field is shown in Figure 11. The susceptibility of the magnetic fluid was 2.44×10^{-5} with its saturation magnetization of 665.4 mT.

Rheological property of magnetic fluid

For the successful application of magnetic fluid, it is very important to obtain its rheological property. The relationship between viscosity and flow rate obtained using a capillary rheometer is shown in Figure 12. It could be seen that the viscosities of magnetic fluid were almost constant at increasing flow rate when the solid concentration was low (5%), indicating that the fluid behaved as Newtonian fluid. In stable magnetic fluid, there is almost no interaction among particles.[14] Seen from the UV–vis absorption curves of magnetic fluid (as shown in Fig. 8), the obtained suspension was stable enough.

Therefore, the interaction among particles can be ignored in dilute suspension, and the fluid viscosity was independent of shear rate.

The rheological behavior derivates the Newtonian fluid when the solid concentration is relative high (>10%). The shear-thinning behavior can be seen clearly when the solid concentration is 17%.

Figure 13 shows the relationship between viscosity and temperature. It is interesting to find that the viscosity of magnetic fluid decreased with the increasing temperature. One possible explanation can be proposed for this result: when temperature increased, Brownian movement of magnetic nanoparticles enhanced, leading to the more probability of particles collisions. Hence, the viscosity of magnetic fluid had the tendency to increase. However, the viscosity of surfactant solution decreased when the temperature increased (as shown in Fig. 13), and this effect played a dominant role. As a whole, the viscosity of magnetic fluid decreased.

Mechanical properties of PVA films

It was revealed in earlier studies[15–19] that the mechanical properties of polymers could be improved by the addition of nanoparticles. In the present
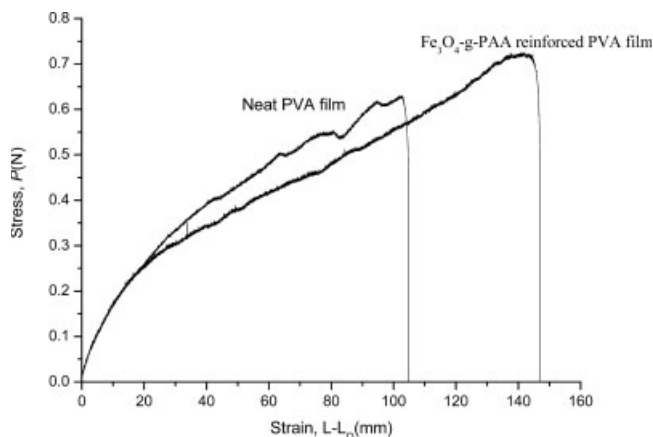

Figure 15 The stress–strain curve of two PVA thin films.

TABLE II
Mechanical Properties of Neat and
Nanoparticle-Reinforced PVA Films

Tensile properties	Neat PVA	Nanoparticle-reinforced PVA
Maximum strength (N)	0.6308	0.7260
Elongation at break (mm)	104.91	146.84

investigation, the mechanical properties of prepared thin films were measured on a tensile tester. The shape of the test samples is shown in Figure 14 while the dimensions are listed in Table I. The SS curve of neat PVA and nanoparticle-reinforced PVA are presented in Figure 15. The curve pattern is affected obviously by the addition of nanoparticles. The figure also illustrates that the presence of nanoparticles increases the tensile strength due to a strong interfacial interaction between hydrophilic PVA and the polar surface of nanoparticles.

Table II shows that significant enhancement in maximum tensile strength is achieved for nanoparticle-reinforced PVA. The enhancement of maximum strength is reasonably attributed to the high resistance exerted by rigid nanoparticles against the plastic deformation as well as the stretching resistance of the polymer chains surrounded by nanoparticles. The elongation to break also increased for the nanoparticle-reinforced PVA.

CONCLUSIONS

In the present investigation, magnetic Fe$_3$O$_4$ nanoparticles, synthesized by coprecipitation, were characterized by various methods. These nanoparticles were used to prepare magnetic fluid and PVA thin film. The following conclusions can be drawn: (1) Acrylic acid was successfully introduced onto the surface of Fe$_3$O$_4$ nanoparticles. The optimum reaction condition was 4 mL of acrylic acid and 130 mg of AIBN at 55°C. (2) Fe$_3$O$_4$ magnetic fluid was synthesized by employing magnetic Fe$_3$O$_4$ nanoparticles as basic substance and water as mediated fluid. The susceptibility of resultant magnetic fluid was 2.44 $\times$ 10^{-5} and the saturation magnetization was 665.4 mT.

In addition, the mean size d (0.98) of magnetic Fe$_3$O$_4$ nanoparticles in the magnetic fluid was 57.42 nm. (3) The obtained magnetic fluid was Newtonian at low concentration, and was non-Newtonian (shear-thinning) at high concentration. The viscosity of magnetic fluid decreased with increasing temperature. (4) The mechanical properties of PVA thin film were greatly enhanced with the addition of Fe$_3$O$_4$ magnetic fluid.

References

1. Mohallem, D. S.; Seara, L. M. Appl Surf Sci 2003, 214, 143.
2. Cao, J. Q.; Wang, Y. X.; Yu, J. F.; Xia, J. Y.; Zhang, C. F.; Yin, D. Z.; Häfeli, U. O. J Magn Magn Mater 2004, 277, 165.
3. Ma, M.; Zhang, Y.; Yu, W.; Shen, H. Y.; Zhang, H. Q.; Gu, N. Colloids Surf A 2003, 212, 219.
4. Bocanegra-Diaz, A.; Mohallem, N. D. S.; Naovak, M. A.; Sinisterra, R. D. J Magn Magn Mater 2004, 272/276, 2395.
5. Khollam, Y. B.; Dhage, S. R.; Potdar, H. S.; Deshpande, S. B.; Bakare, P. P.; Kulkarni, S. D.; Date, S. K. Mater Lett 2002, 56, 571.
6. Bica, I. Mater Sci Eng B 1999, 68, 5.
7. Chen, G. X.; Hong, M. H. Appl Surf Sci 2004, 228, 169.
8. Shchukin, D. G.; Radtchenko, I. L.; Sukhorukov, G. B. Mater Lett 2003, 57, 1743.
9. Bae, D. S.; Han, K. S.; Cho, S. B.; Choi, S. H. Mater Lett 1998, 37, 255.
10. Rheinlander, T.; Priester, T. J Magn Magn Mater 2003, 256, 252.
11. Qian, J. Z.; Hong, R. Y. Chem Res 2004, 15, 18 (in Chinese).
12. Implementation Main Points of China National Standard GB/T228-2002, available at: http://www.instrument.com.cn/bbs/shtml/20051214/300437/ (in Chinese).
13. Rosensweig, R. E. Ferrohydrodynamics; Dover: Mineola, NY, 1998; p 136.
14. Berkovsky B. M.; Medvedev, V. F. Magnetic Fluids Engineering Applications; Oxford University Press: Oxford, 1993.
15. Chae, D. W.; Kim, B. C. Polym Adv Technol 2005, 16, 846.
16. Chae, D. W.; Kim, B. C. J Appl Polym Sci 2006, 99, 1854.
17. Zheng, Y. P.; Zheng, Y.; Ning, R. C. Mater Lett 2003, 57, 2940.
18. Tillekeratne, M.; Jollands, M.; Cser, F.; Bhattacharya, S. N. J Appl Polym Sci 2006, 10, 2652.
19. Bikiaris, D. N.; Papageorgiou, G. Z.; Pavlidou, E.; Vouroutzis, N.; Palatzoglou, P.; Karayannidis, G. P. J Appl Polym Sci 2006, 10, 2684.